Fluorescence Properties of a New Guanosine Analog Incorporated into Small Oligonucleotides

Sarah L. Driscoll,* Mary E. Hawkins,# Frank M. Balis,# Wolfgang Pfleiderer,§ and William R. Laws*
*Department of Biochemistry, Mount Sinai School of Medicine, New York, New York, 10029, and #Pediatric Branch, National Cancer Institute, Bethesda, Maryland, 20892 USA; and §Fakultät für Chemie, Universität Konstanz, D-78464 Konstanz, Germany

ABSTRACT The fluorescence properties of 3-methyl-isoxanthopterin (3-MI) incorporated into different oligonucleotides have been determined. This highly fluorescent guanosine analog has its absorption and fluorescence spectra well resolved from those of the normal nucleotides and the aromatic amino acids. The small shifts observed in absorption and fluorescence emission spectra upon incorporation of 3-MI into these oligonucleotides are consistent with a general solvent effect and do not suggest any contribution from the position of the probe from the 5′ end, the sequence of nucleotides immediately 5′ or 3′ to the probe, or the single- or double-stranded nature of the oligomer. However, steady-state and time-resolved fluorescence studies indicate that the presence of a purine immediately 5′ or 3′ to the probe results in some dynamic but mostly static quenching in the single-stranded oligomer. Furthermore, a 3′ purine is more effective than a 5′ purine, and an adenine appears to be more effective than a guanine for these static quenching interactions. Formation of the double-stranded oligomer leads to an additional loss of quantum yield, which can also be ascribed primarily to static quenching. These results show that this new class of spectrally enhanced fluorescent purine analogs will be able to provide useful information concerning the perturbation of nucleic acid structures.

INTRODUCTION

Examination of the structure and dynamics of protein-DNA complexes should provide important information about how these macromolecules interact and function. Fluorescence spectroscopic techniques can be extremely useful as specific sites in both the protein and the nucleic acid can be examined and as the studies can be performed under physiological conditions, especially with respect to concentration. Although extrinsic fluorescent probes can be useful, through either a covalent attachment or a noncovalent interaction, it is preferable to use naturally occurring chromophores or related analogs as intrinsic fluorophores to minimize any possibility of perturbation induced by an outside agent.

The use of naturally occurring chromophores to study protein-DNA interactions has its limitations. For example, it is difficult to use fluorescence spectroscopy for solution studies of nucleic acid structure, function, and dynamics. The usual bases all have very low fluorescence quantum yields as well as similar absorption and emission spectra (Konev, 1967). As a result, sensitivity is low and it is difficult to know which base absorbs and/or emits the light. Although protein structure, function, and dynamics have been extensively studied in solution by the fluorescence of tryptophan residues (Beechem and Brand, 1979), it becomes difficult to interpret results when there are more than one protein involved, each with one or more tryptophan residues. Furthermore, the large extinction of the nucleic acids, even at 295 nm, effectively filters the light meant to excite the tryptophans in a protein-DNA complex.

Recently, tryptophan analogs with an absorption band at lower energies (red-shifted) than that of tryptophan have been shown to be very useful in examining protein-protein and protein-DNA complexes (Hogue et al., 1992; Ross et al., 1992, 1997). This spectral enhancement allows these analogs to be exclusively excited for fluorescence studies even when in the presence of DNA or other tryptophan-containing proteins. In analogy with proteins, therefore, a possible approach to help study protein-DNA complexes from the perspective of the DNA is to employ base analogs that have different spectral properties and higher fluorescence quantum yields. One base analog that has been previously examined in short oligonucleotides (oligos) is 2-aminopurine (2-AP) (Nordlund et al., 1989; Guest et al., 1991; Hochstrasser et al., 1994), which is able to form hydrogen bonds with either thymine or cytosine.

To facilitate fluorescence studies involving oligos, it would be useful to have a series of spectrally enhanced fluorescent nucleotide analogs to permit replacement of any nucleotide while maintaining all aspects of oligo structure, including recognition sites for protein binding. By the systematic replacement of specific nucleotides, this set of analogs should help elucidate the changes in nucleic acid structure and dynamics that result from interactions with other biomolecules. To address this need, a new class of fluorescent nucleotide analogs has been developed that not only absorb at UV wavelengths well resolved from those

Received for publication 20 December 1996 and in final form 21 August 1997.

Address reprint requests to Dr. William R. Laws, Department of Biochemistry, Mount Sinai School of Medicine, One Gustave L. Levy Place, New York, NY 10029. Tel.: 212-241-6545; Fax: 212-996-7214; E-mail: wlaws@smtplink.mssm.edu.

S. L. Driscoll's present address: Department of Bioengineering, University of California at San Diego, La Jolla, CA 92093.

0006-3495/97/12/3277/10 $2.00

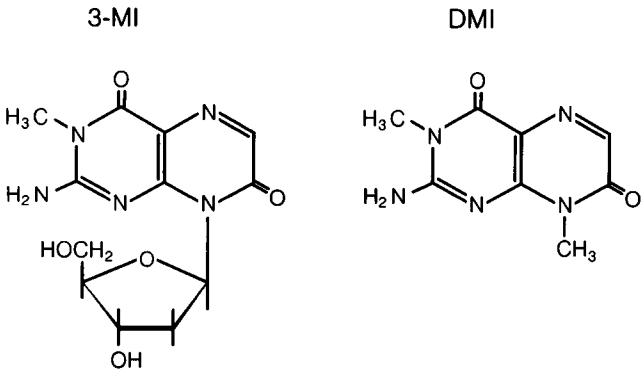

FIGURE 1 The chemical structures of 3-methyl-8-(2-deoxy-β-D-ribofuranosyl) isoxanthopterin (3-MI) and 3,8-dimethylisoxanthopterin (DMI).

absorbed by the usual nucleotides and the aromatic amino acids but also have significant quantum yields (Hawkins et al., 1997). One of these probes, the guanosine analog 3-methyl-8-(2-deoxy-β-D-ribofuranosyl) isoxanthopterin (3-MI), is depicted in Fig. 1. Interestingly, it is the extra carbonyl group at position 7 of the isoxanthopterin ring system that results in the absorption and fluorescence spectral shifts as well as the increased quantum yield.

In this report, we present steady-state and time-resolved fluorescence studies performed on 3-MI free in solution and when incorporated at various positions into single-stranded (ss) and double-stranded (ds) oligos of different lengths and sequences. The results suggest that 3-MI in a ss oligo can form ground-state complexes, particularly with purines immediately 5′ or 3′ of the probe, and these complexes significantly reduce the fluorescence quantum yield by static quenching processes. The additional loss of quantum yield on formation of the ds oligo can also be shown to be primarily a result of interactions leading to static quenching. These effects should allow an evaluation of the ss/ds nature of the region of the oligo containing the analog.

MATERIALS AND METHODS

Unless stated otherwise, all chemicals used in these studies were reagent grade and all experiments were performed at 20°C. The standard buffer was 10 mM Tris, pH 8, with 75 mM KCl and 1 mM EDTA.

Samples

Table 1 gives the sequences of the oligos used in this study; these oligos permit an evaluation of the fluorescence properties of 3-MI as a function of oligo length, position from the 5′ end, and neighboring nucleotides. These oligos were synthesized using an Applied Biosystems model 392 (Foster City, CA) automated DNA synthesizer. The details of the synthesis, including the preparation of 3-MI phosphor-amidite, the incorporation of 3-MI into an oligo, and the purification of the ss oligo as well as an extinction coefficient and other spectroscopic properties of 3-MI have been previously reported (Hawkins et al., 1995). Oligo strands complementary to those listed in Table 1, with a cytosine incorporated to complement the 3-MI probe, were similarly synthesized and purified.

The ss 3-MI-containing oligomers were annealed with their complement strands. An equal molar mixture of the 3-MI-containing strand and its complement was incubated in a 75°C water bath for 10 min. The water bath, with the sample still immersed, was then packed in styrofoam and placed in a 37°C incubator. The temperature of the water bath reached that of the incubator after 5 h. At this time, the sample was removed from the bath/incubator and allowed to cool to room temperature. The annealed, ds material was then purified by fast performance liquid chromatography (Pharmacia Biotech, Piscataway, NJ) at either 4°C or room temperature (~22°C) using a MonoQ ion exchange column (Pharmacia Biotech HR 10/10). The sample was loaded onto the column that was previously equilibrated with standard buffer and then eluted with a linear gradient of 0.25 to 0.75 M KCl over 50 ml. The elution volume for each oligo was length dependent, with elution for the 21-base-pair oligos occurring near 0.62 M KCl. Fractions containing the ds material were combined and then desalted into standard buffer and concentrated using a Centricon 3 (Amicon, Beverly, MA). The 3-MI-containing ds samples exhibited the expected electrophoretic mobilities in a 20% polyacrylamide gel when compared with the mobilities for ds oligos of known length.

The corresponding base with a methyl group instead of the deoxyribose moiety, 3,8-dimethyl-isoxanthopterin (DMI) (see Fig. 1), was also prepared (Pfleiderer and Rukwied, 1961). DMI was studied to determine the effect of the deoxyribose group on the spectroscopic properties of 3-MI.

TABLE 1 3-MI-containing oligonucleotides

Oligo	Length	Position*	Sequence (5′ to 3′)
EcoR1	21	4	agt **F**aa ttc gcc ctt cca gtg
Pter2	21	5	gtg t**F**g aaa atc tct agc agt
Pter18	21	7	act gct **F**tc gat ttt cca cac
BL-3	21	7	act act **F**tc act gat cag cac
Pter7	21	10	act gct aga **F**at ttt cca cac
PCR6	19	10	tct ctc gaa **F**ag ccc gct c
PCR4	19	10	att cca caa **F**gc cgt gtc a
PCR7-1	19	10	acc gct gaa **F**ga gga agc a
SK38P3	30	11	gat gac aaa g**F**c taa tcc acc tat ccc cgt
BL-2	18	13	att cca caa gcc **F**tg tca
BL-1	20	14	acc gct gaa gga g**F**g aag ca
Pter4	21	17	gtg tgg aaa atc tct a**F**c agt
HP-5	33	17	cct cta aga ggt gtc c**F**c ctg tgg aga atc tcc

F represents the 3-MI analog.
*Position of the 3-MI nucleotide analog numbering from the 5′ end.

Spectroscopy

Optical densities and absorption spectra of samples were obtained at room temperature using a Hitachi U-3210 UV/Vis dual beam spectrophotometer. Spectra were digitally transferred from the spectrometer to a computer for data analysis and graphics.

Fluorescence experiments were carried out in 4 × 10 mm path-length quartz cuvettes, with excitation along the 10-mm axis, on samples having absorbances ≤0.05 at the excitation wavelength. Steady-state fluorescence measurements of uncorrected spectra, relative quantum yields, anisotropy, and quenching were obtained using an SLM/Aminco SPF 500C spectrofluorimeter. The bandpasses for the excitation and emission monochromators were 4 nm. Relative quantum yields were estimated by comparing the areas of emission spectra, which had been obtained under the same optical conditions, normalized to equivalent optical densities at the excitation wavelength. Fluorescence quenching experiments were performed by adding small aliquots of 1 M acrylamide (Serva, New York, NY; four times recrystallized) dissolved in standard buffer. The quenching data were corrected for dilution and then evaluated using the Stern-Volmer equation (Stern and Volmer, 1919), $F_o/F = 1 + K_{SV}$ [Q], where F_o and F are the fluorescence intensities in the absence and presence of the quencher Q, respectively. The Stern-Volmer constant, K_{SV}, is equal to $k_q\tau_o$ where k_q is the bimolecular quenching rate constant and τ_o is the lifetime of the fluorophore in the absence of quencher. The excitation and emission wavelengths were 350 and 430 nm, respectively, for the quenching and anisotropy experiments.

To obtain the principal polarization spectrum of 3-MI, an aliquot of 3-MI dissolved in ethanol was dried in a flask and redissolved in glycerol (Mallinckrodt, Paris, KY; analytical grade; lot 5092 KLNY had no background fluorescence under the conditions used in these experiments). Fluorescence intensity was monitored at 430 nm on an SLM 4800 spectrofluorimeter modified for photon counting, with excitation and emission bandpasses of 2 and 4 nm, respectively. Four excitation scans were collected from 270 to 400 nm, with the excitation and emission polarizers in the vv, vh, hh, and hv positions, where the first/last letter denotes the position of the excitation/emission polarizer and v represents the vertical and h the horizontal orientations of each polarizer. The steady-state anisotropy, ⟨r⟩, was then calculated as $\{(I_{vv} - G \times I_{vh})/(I_{vv} + 2G \times I_{vh})\}$, where the instrument correction factor $G = I_{hv}/I_{hh}$ and I_{xy} represents the fluorescence intensities for each designated set of polarizer orientations.

Time-resolved fluorescence experiments were done by the time-correlated, single-photon counting method using a fluorimeter that has been described in detail (Hasselbacher et al., 1991). Samples were excited with vertically polarized 323- or 335-nm light by a frequency-doubled, cavity-dumped (4.1 MHz) dye laser, using either a rhodamine (R6G) or a coumarin (DCM) dye that was pumped by a mode-locked (82 MHz), frequency-doubled Nd-YAG laser. Emission wavelengths were selected by a Jobin-Yvon (100 mm) monochromator with a bandpass of 20 nm. Decay curves were collected into 2000 or 4000 channels, with respective timing resolutions of 22 and 11 ps/channel. The instrument response function, obtained by light scattering, was typically collected to a minimum of 100,000 counts in the peak channel whereas decay curves were collected to a minimum of 40,000 counts in the peak channel.

Fluorescence decay data were analyzed by a reconvolution procedure (Grinvald and Steinberg, 1974) using nonlinear least-squares regression (Bevington, 1969). Intensity decays, $I_m(t)$, collected through an emission polarizer set at the magic angle (Lakowicz, 1983), were fit to a sum of n exponentials:

$$I_m(t) = \sum_{i=1}^{n} \alpha_i e^{-t/\tau_i} \quad (1)$$

where α_i and τ_i are the amplitude and lifetime of the ith component, respectively. To obtain the parameters describing the decay of the emission anisotropy, r(t), a decay curve obtained with a vertically-oriented emission polarizer, $I_v(t)$, and a decay curve obtained with a horizontally-oriented emission polarizer, $I_h(t)$, were analyzed simultaneously with $I_m(t)$ (Waxman et al., 1993) using the following expressions:

$$I_v(t) = \frac{I_m(t)}{3}\left(1 + 2\sum_{j=1}^{k} \beta_j e^{t/\phi_j}\right) \quad (2)$$

$$I_h(t) = \frac{I_m(t)}{3}\left(1 - \sum_{j=1}^{k} \beta_j e^{-t/\phi_j}\right) \quad (3)$$

where ϕ_j terms are the rotational correlation times. The β_j terms are dependent on several factors, including the orientation of the excitation and emission dipole moments of the fluorophore with respect to each other and the rotational axes of the macromolecule. The time 0 anisotropy, r_o, is defined as $\Sigma\beta_j$. All fits were judged by the reduced χ^2, the weighted residuals, and the autocorrelation of the residuals. The steady-state anisotropy, ⟨r⟩, was applied in some r(t) analyses to scale $I_v(t)$ and $I_h(t)$ (Badea and Brand, 1979).

RESULTS AND DISCUSSION

Spectral analysis

The lowest-energy electronic absorption band of 3-MI dissolved in buffer is shown in Fig. 2 *A*. The maximum is near 350 nm, well separated in energy from the absorption bands

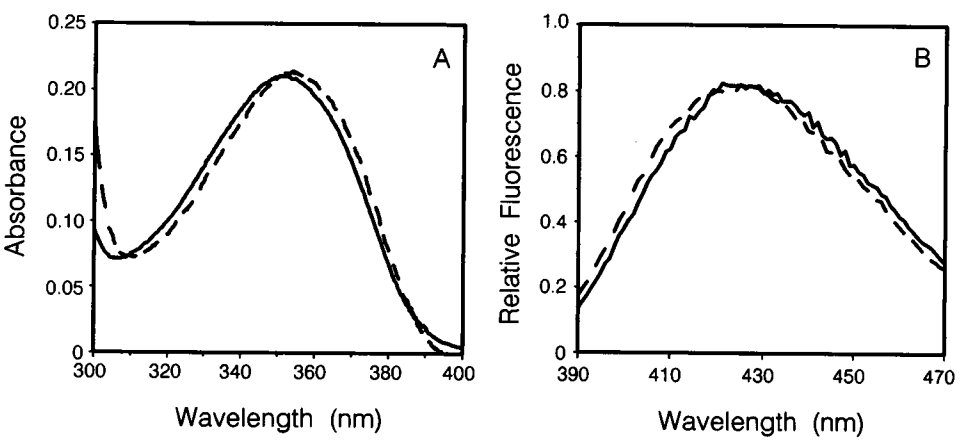

FIGURE 2 Spectra for 3-MI (——) and 3-MI incorporated into ss Pter18 (---), both dissolved in the standard buffer. (*A*) Absorption spectra. (*B*) Peak normalized, uncorrected fluorescence emission spectra.

of the usual nucleotides and the aromatic amino acids. Also displayed in Fig. 2 *A* is the same absorption band for the ss form of oligo Pter18; concentrations were adjusted to match peak absorbances and thus facilitate a comparison. Although a small shift to lower energies (red-shift) is observed with Pter18, there are no perturbations in the shape of its spectrum with respect to the 3-MI spectrum. The absorption spectra for the other ss oligos and all of the ds oligos are similar to that seen for Pter18 and are therefore not shown. Several of the ds oligos, however, exhibit an additional small red shift compared with their corresponding ss oligos. The absorption maxima for all samples are listed in Table 2 and are in agreement with other 3-MI-containing oligos previously examined (Hawkins et al., 1995, 1997). It can be concluded, therefore, that the energies of light absorbed by the analog are not affected to any significant extent by: 1) the length of the oligo, 2) the position of the 3-MI chromophore relative to the 5′ end, or 3) the sequence of nucleotides immediately 5′ or 3′ of the probe. The additional small shift in absorption maxima observed for some of the ds oligos also does not correlate with the above three factors. The small shift to lower absorption energies observed with the ss oligos, and the additional small shift seen with several of the ds oligos, however, is characteristic of many aromatic chromophores entering an environment less polar than that of water (Cantor and Schimmel, 1980). Thus, it appears that the analog is less exposed to solvent when it is incorporated into a polynucleotide chain.

TABLE 2 Steady-state fluorescence parameters

Nearest neighbors (5′ to 3′)	Sample		Absorption maximum (nm)	Emission maximum (nm)	Φ*
—	DMI		344	413	ND
—	3-MI		350	425	1
-Pyr-(3-MI)-Pyr-	Pter18	(ss)	354	421	0.33
		(ds)	355	422	0.03
	BL-3	(ss)	354	423	0.53
		(ds)	360	421	0.06
	BL-2	(ss)	355	424	0.24
		(ds)	359	423	0.014
	HP-5	(ss)	356	426	0.25
		(ds)	360	427	0.008
-Pyr-(3-MI)-Pur-	EcoR1	(ss)	355	425	0.03
		(ds)	354	425	0.02
	Pter2	(ss)	356	424	0.025
		(ds)	356	427	0.007
-Pur-(3-MI)-Pyr-	Pter4	(ss)	355	422	0.08
		(ds)	356	423	0.03
	SK38P3	(ss)	355	425	0.08
		(ds)	360	421	0.015
-Pur-(3-MI)-Pur-	Pter7	(ss)	356	426	0.006
		(ds)	357	425	0.005
	PCR6	(ss)	356	426	0.014
		(ds)	359	427	0.026
	PCR4	(ss)	355	425	0.027
		(ds)	360	426	0.012
	PCR7-1	(ss)	354	424	0.025
		(ds)	359	425	0.006
	BL-1	(ss)	357	424	0.032
		(ds)	360	421	0.005

ND, not determined.
*Quantum yield relative to 3-MI.

As shown in Fig. 2 *B*, the fluorescence emission spectrum of 3-MI in buffer is a broad, structureless band with a maximum (uncorrected) near 425 nm. Fig. 2 *B* also shows that the emission spectrum of 3-MI incorporated into ss Pter18 resembles the spectrum for 3-MI free in solution with no changes in the shape of the emission spectrum. The emission spectra for all of the other ss and ds oligos (not shown) essentially overlay the spectrum of ss Pter18, including the small shift to higher energies (blue-shift) observed for 3-MI in an oligo compared with 3-MI in solution. Maximal wavelengths for the fluorescence emission of the various samples are given in Table 2; these values are consistent with those for other 3-MI-containing oligos previously examined (Hawkins et al., 1997). As discussed above for the small absorption shift, the small blue-shift in the emission spectra of 3-MI in the oligos suggests that the fluorophore is in a less polar environment (Lakowicz, 1983). In addition, in direct analogy with the absorption results, it appears that the energy of the excited state is not affected to any significant extent by 1) the length of the oligo, 2) the position of the 3-MI probe relative to the 5′ end, 3) the sequence of nucleotides immediately 5′ or 3′ of the probe, or 4) the ss or ds state of the oligo.

The energy shifts in absorbance and emission observed for 3-MI incorporated into these short oligos suggest that the fluorophore is in a different environment than that experienced by 3-MI in solution. The magnitude of these shifts, however, is small. As a consequence, it would be difficult to use these spectral shifts to evaluate the polar nature of the local environment for 3-MI in an oligo similar to the way that different environments have been established for tryptophan residues in a protein (Eftink, 1991). In combination with the insensitivity of the spectra with respect to oligo length, analog position, neighboring nucleotides, and ss or ds forms, these small spectral shifts are not an effective way to assess the local environment of this nucleotide analog. However, the absorption and emission maxima of near 350 and 425 nm, respectively, demonstrate the possible advantages of using 3-MI and related analogs (Hawkins et al., 1997) as spectroscopic probes of nucleic acid structure and function. Besides its own capabilities as a probe, the large spectral overlap between the emission spectrum of a Trp residue (or Trp analog) and the absorption spectrum of 3-MI suggests that resonance energy transfer experiments could be used to help evaluate protein-DNA interactions.

Quantum yields

The fluorescence quantum yield of 3-MI dissolved in a 10 mM Tris, pH 7.5 buffer has been reported to be 0.88 relative to quinine sulfate in 0.1 N sulfuric acid (Hawkins et al., 1995). Upon incorporation into oligos, however, its quan-

tum yield decreases (Hawkins et al., 1995, 1997). The fluorescence quantum yield of 3-MI when incorporated into all of the ss oligos listed in Table 1 is also reduced, ranging from 0.006 to 0.53 compared with 3-MI in standard buffer, which has been assigned a relative quantum yield of unity. In an attempt to assess the cause(s) of this wide range of values, a bar graph was generated (Fig. 3) arranging the oligos in order of increasing fluorescence quantum yield. Various factors were then examined to explain the results. The position of the probe within the oligo, relative to the 5′ end, does not appear to affect the quantum yield; this has been noticed previously in other 3-MI-containing oligos (Hawkins et al., 1997). In addition, a correlation between oligo length and quantum yield is not apparent.

As indicated in Fig. 3, all nine of the ss oligos with a quantum yield less than 0.1 have a purine immediately 5′ or 3′ of the chromophore. Furthermore, based on Pter4 and SK38P3, a 3′ purine appears to attenuate the quantum yield more than a 5′ purine does. Interestingly, the lowest fluorescence quantum yields are found with adenine both 5′ and 3′ of the probe. When both the 5′ and 3′ nearest neighbors are pyrimidines, a significant increase in quantum yield is observed, with thymidine perhaps permitting a higher quantum yield than cytosine. The larger fluorescence quantum yield for BL-3 compared with Pter18, both of which have 5′ and 3′ thymidines and are 21-mers with the probe at position 7, is difficult to assess. Although it has been reported that the second nearest neighboring bases can have a small effect on the quantum yield (Hawkins et al., 1997), they are the same in BL-3 and Pter-18. All of the fluorescence quantum yields for the ss oligos have also been listed in Table 2, which has been organized into four groups based on the type of nucleotides (purine or pyrimidine) immediately 5′ and 3′ of the 3-MI probe.

Formation of the ds oligo results in a further reduction in quantum yield. The extent of this effect depends on the type of nucleotides immediately 5′ and 3′ to the 3-MI. For those oligos of type -Pyr-(3-MI)-Pyr in Table 2, there is at least an order of magnitude loss in quantum yield between the ss and the ds forms. A much smaller effect is found for the oligos in the other three classes in Table 2, but those already had significantly lower quantum yields for the ss oligos due to the presence of one or more purines. As a result of this differential sequence effect on quantum yield upon going from a ss to a ds oligo, the hierarchy observed above for the quantum yield of 3-MI changes slightly as shown in Fig. 4. Although the overall trend of neighboring purines is maintained, especially when 3′ of 3-MI, there are some exceptions. For example, HP-5, BL-2, EcoR1, and PCR6 now have different places in the quantum yield ranking of the oligos.

The reason for this realignment of the oligos with respect to their relative fluorescence quantum yields is not immediately apparent. Although experimental error could play a role, especially as these quantum yields are quite small, repeated quantum yield determinations have indicated that variations between measurements are an order of magnitude smaller than variations between different oligos. When determining a relative quantum yield for an oligo, there may also be an effect from neighboring bases on the absorbance of the probe (Brown and Brown, 1991). The shielding of absorbance by neighboring bases could influence the accuracy of the absorbance measurement, which is critical for a quantum yield determination, and this could cause small differences in quantum yields for a fluorescent nucleotide analog in similar oligos. It is quite clear, however, that the large differences in quantum yields resulting from whether a purine or a pyrimidine is 5′ and/or 3′ of the 3-MI probe is not a result of this absorbance shielding effect.

Similar fluorescence quantum yields have been reported for other 3-MI-containing ss and ds oligos (Hawkins et al., 1997). However, the large decrease upon ds formation for

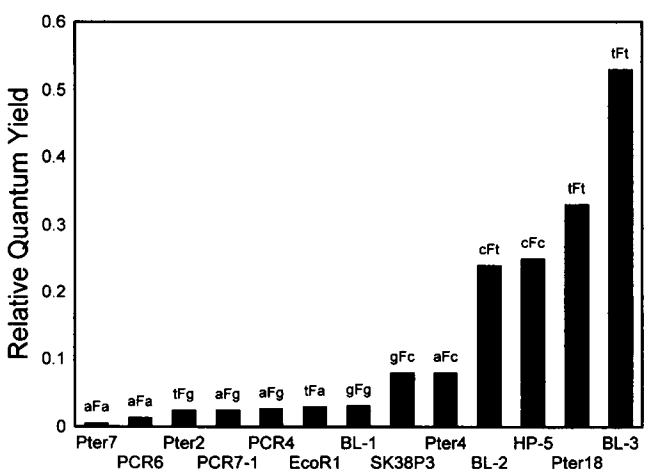

FIGURE 3 The relative fluorescence quantum yields (Table 2), arranged by increasing magnitude, for the ss oligos listed in Table 1. Each oligo is labeled with the three nucleotides centered around the 3-MI probe depicted by F.

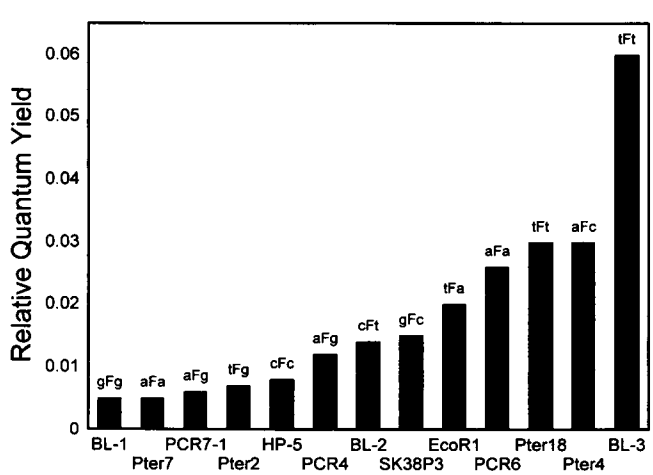

FIGURE 4 The relative fluorescence quantum yields (Table 2), arranged by increasing magnitude, for the ds oligos listed in Table 1. Each oligo is labeled with the three nucleotides centered around the 3-MI probe depicted by F.

several of the samples has not been seen previously. To test this ss→ds effect on quantum yield, a qualitative DNA melting experiment (not shown) was performed on the Pter18 ds sample. A large increase (~five times) in fluorescence intensity was observed upon raising the solution temperature slowly from 25 to 75°C. This is consistent with the release of quenching induced by ds formation; the full quantum yield effect was not observed due to the adverse effect of higher temperatures on fluorescence quantum yields. The T_m was estimated to be in the 50–60°C range, in agreement with melting temperatures previously determined by calorimetry for other 3-MI-containing 21-base-pair oligos (Hawkins et al., 1997). Therefore, because the fluorescence quantum yield can change between ss and ds oligos, 3-MI could be used as a sensitive monitor for site-specific ds→ss transitions.

Hawkins et al. previously noted this nearest-neighbor purine effect (Hawkins et al., 1995, 1997) and have shown that it can be applied to the monitoring of DNAse-like activities (Hawkins et al., 1995). They demonstrated that the 3′ processing activity of HIV integrase can be easily assayed by the use of a synthetic oligo substrate that contains 3-MI. The substrate was constructed to be cleaved between 3-MI and its 5′ purine neighbor with release of a dinucleotide product containing the 3-MI. Cleavage of the DNA was measured by the increase in fluorescence resulting from the release of the 5′ purine quenching effect. Consequently, 3-MI not only can be used to provide biophysical parameters as observables to help examine macromolecular interactions but also can be a practical probe to facilitate sensitive biochemical assays.

The environment seen by the 3-MI probe within an oligo must be responsible for the loss of fluorescence intensity. In general, there are two ways the local environment could affect the fluorescence quantum yield. First, the quenching mechanism(s) inherent in chemical groups such as a phosphate from the oligo could add to the nonradiative processes that de-energize the excited state without the emission of a photon. This would be a kinetic process resulting in a reduced fluorescence lifetime for 3-MI in an oligo compared with 3-MI in solution. Second, the isoxanthopterin ring system could be forming a ground-state complex with one or more potential quenching groups. For example, the neighboring purine effect on quantum yields could be the result of base-stacking interactions. Although a photon could still be absorbed, the energy would be instantly lost to the complex. This is an example of static quenching that will not result in a reduced fluorescence lifetime. Consequently, to differentiate between these two possible mechanisms, time-resolved fluorescence intensity decay studies must be performed.

Fluorescence intensity decay

As shown in Table 3, the first excited singlet state of 3-MI in buffer decays as single exponential with a lifetime near 6.5 ns. When incorporated into oligos, however, the fluorescence intensity decay of 3-MI becomes more complex, requiring up to four exponentials to fit the intensity decays of the ss and ds oligos examined here (Table 3). The intensity decay of one sample, the ds form of BL-3, can be described by a sum of three exponentials. Previous work has reported a sum of three exponentials for the decay of 3-MI in other oligos (Hawkins et al., 1997). It should be emphasized, however, that the use of three or four exponential terms to define the fluorescence intensity decays of the ss and ds oligos containing a single 3-MI probe does not suggest a kinetic mechanism. A sum of exponentials is merely a convenient way to approach the analyses; the combination of nonradiative and radiative events may not even result in an exponential decay process (Lakowicz, 1983). More studies will be required to elucidate the kinetic scheme controlling the fluorescence intensity decay of 3-MI incorporated into an oligo. It is very interesting to note that there is a similar increase in the complexity of the fluorescence intensity decay of 2-AP upon its incorporation into an oligo (Nordlund et al., 1989; Guest et al., 1991; Hochstrasser et al., 1994). Furthermore, the magnitudes of the lifetimes and their associated amplitudes are similar between the two nucleotide analogs. A study is underway to examine whether the similar intensity decay patterns seen for both 3-MI and 2-AP upon introduction into an oligo are a result of a similar process or processes.

Although there are variances between corresponding amplitude and lifetime terms listed in Table 3 among the various ss oligos, some generalities can be made. First, the different lifetimes are all within the same range of values: ~0.1, ~0.5, 1–2, and ≥5 ns. Second, the sum of the amplitude terms for the two shortest lifetimes is >0.5 when there is a 3′ purine (except for the oligos BL-1 and PCR7–1). For those oligos with a 3′ pyrimidine, the amplitudes for the two longer lifetimes dominate. Third, the exponential component with the longest lifetime is the largest contributor to the fluorescence intensity decay.

Some changes in intensity decay parameters were observed after formation of the ds oligos (Table 3). Surprisingly, knowing the reduction in the quantum yields, the lifetimes changed very little and often demonstrated a slight increase. With some oligos, there was a dramatic increase in the amplitudes for the shorter lifetimes at the expense of the amplitudes for the longer lifetimes. However, this was not seen for all oligos nor can it be categorized based on the type of nucleotide immediately 5′ and 3′ of the probe.

In the absence of a known kinetic mechanism to account for each amplitude and lifetime, a comparison of average lifetimes is often informative. Both the number-average and the intensity-average lifetimes have been calculated (see Table 3 for their definitions). The number-average lifetime, $\bar{\tau}$, represents the area under the decay curve and is therefore related to quantum yield (Lakowicz, 1983). The intensity-average lifetime, $\langle\tau\rangle$, accounts for the fact that certain excited-state events, such as a dynamic quenching interaction, are time dependent and are therefore proportional to the

TABLE 3 Time-resolved fluorescence intensity decay parameters

Sample*		α_1#	α_2	α_3	α_4	τ_1 (ns)	τ_2 (ns)	τ_3 (ns)	τ_4 (ns)	$\%f_1$§	$\%f_2$	$\%f_3$	$\%f_4$	$\bar{\tau}$ (ns)‖	$\langle\tau\rangle$ (ns)¶
DMI		1.0				5.9									
3-MI		1.0				6.5									
Pter18	(ss)	0.14	0.19	0.26	0.41	0.2	1.1	2.7	5.2	1.0	6.6	22.9	69.4	3.1	4.3
	(ds)	0.36	0.58	0.03	0.03	0.2	0.5	2.0	6.6	11.8	49.0	8.9	30.3	0.7	2.5
BL-3	(ss)	0.07	0.13	0.23	0.57	0.1	0.7	2.7	5.9	0.2	2.3	15	82.5	4.1	5.3
	(ds)**	0.49	0.49		0.02	0.3	0.8		5.1	25.1	61.2		13.7	0.7	1.3
BL-2	(ss)	0.19	0.19	0.36	0.26	0.2	1.0	2.8	5.0	1.6	7.2	39.9	51.3	2.5	3.8
	(ds)	0.59	0.26	0.06	0.09	0.2	0.5	2.1	5.3	11.7	16.8	14.7	56.8	0.8	3.4
HP-5	(ss)	0.25	0.12	0.17	0.46	0.1	0.6	3.2	6.4	0.7	2.2	15.4	81.7	3.6	5.8
	(ds)	0.71	0.11	0.07	0.11	0.08	0.4	2.0	5.9	6.3	5.5	15.1	73.1	0.9	4.6
EcoR1	(ss)	0.53	0.20	0.16	0.11	0.09	0.6	2.0	4.6	4.8	11.2	31.1	52.9	1.0	3.1
	(ds)	0.83	0.12	0.03	0.02	0.1	0.4	2.1	6.1	33.3	14.3	14.7	37.7	0.4	2.7
Pter2	(ss)	0.29	0.31	0.27	0.13	0.1	0.6	1.8	4.0	2.5	14.3	39.7	43.5	1.2	2.6
	(ds)	0.41	0.26	0.13	0.20	0.2	0.7	2.5	6.0	4.2	9.5	18.3	68.0	1.8	4.6
Pter4	(ss)	0.39	0.16	0.21	0.24	0.1	0.7	2.9	5.5	2.0	5.1	29.1	63.8	2.1	4.4
	(ds)	0.80	0.13	0.02	0.05	0.1	0.4	2.1	5.8	21.3	9.5	9.5	59.7	0.5	3.7
SK38P3	(ss)	0.26	0.15	0.27	0.32	0.07	0.6	2.7	4.9	0.7	3.8	31.3	64.2	2.4	4.0
	(ds)	0.12	0.27	0.32	0.29	0.3	1.2	3.2	6.7	0.9	9.4	30.5	59.2	3.3	5.0
Pter7	(ss)	0.64	0.11	0.08	0.17	0.06	0.5	2.3	5.5	3.4	4.5	15.1	77	1.2	4.6
	(ds)	0.74	0.14	0.06	0.06	0.07	0.6	2.4	6.7	7.8	11.4	22.9	57.9	0.7	4.5
PCR6	(ss)	0.77	0.12	0.05	0.06	0.06	0.3	1.7	4.7	10.4	8.0	19.7	61.9	0.4	3.3
	(ds)	0.78	0.19	0.02	0.01	0.08	0.2	0.9	4.0	40.7	21.3	8.5	29.5	0.2	1.3
PCR4	(ss)	0.54	0.13	0.14	0.19	0.06	0.5	2.3	5.2	2.3	4.6	22.7	70.4	1.4	4.2
	(ds)	0.40	0.09	0.09	0.42	0.2	0.9	3.2	6.6	2.1	2.4	9.4	86.1	3.2	6.0
PCR7-1	(ss)	0.21	0.17	0.30	0.32	0.1	0.7	2.7	5.2	0.9	4.6	30.9	63.6	2.7	4.2
	(ds)	0.50	0.11	0.09	0.30	0.1	0.7	2.6	6.4	2.6	3.1	10.7	83.6	2.3	5.6
BL-1	(ss)	0.13	0.17	0.22	0.48	0.2	0.7	2.8	5.5	0.6	3.5	18.5	77.4	3.4	4.8
	(ds)	0.26	0.25	0.32	0.17	0.3	1.4	4.6	7.3	2.8	10.7	47.2	39.3	3.1	5.2

*Samples grouped by nearest neighbors; see Table 2.
#Amplitudes normalized to a sum of 1.
§The percent contribution of each exponential component to the total fluorescence intensity: $100 \times (\alpha_i\tau_i/\Sigma\alpha_i\tau_i)$.
‖The number-average lifetime: $\Sigma\alpha_i\tau_i/\Sigma\alpha_i$.
¶The intensity-weighted lifetime: $\Sigma\alpha_i\tau_i^2/\Sigma\alpha_i\tau_i$.
**Aligned by lifetime values.

individual fluorescence lifetimes. Bar graphs were then constructed for each set of average lifetimes, consisting of both ss and ds data but in increasing order with respect to the ss oligos; the intensity average lifetimes are displayed in Fig. 5. There is no obvious relationship of 3-MI position or oligo length to the intensity average lifetimes. In addition, the groupings based on nucleotide sequence seen with the quantum yields (Fig. 3) do not apply to Fig. 5. There are also not any obvious correlations between ss and ds intensity-average lifetimes, especially as some decrease, some increase, and others are insensitive to the ss or ds status of the oligo. A similar inability to find relationships is found with the number-average lifetimes (not shown). Consequently, an examination of either average lifetime does not provide any correlations with respect to the location of the 3-MI probe in the oligo nor the length or sequence of the oligo.

An important observation is that, although both average lifetimes for 3-MI in each oligo are less than those for 3-MI in solution, neither the number-average nor the intensity-average lifetime for each sample decreased to the same extent that their relative quantum yields did (Tables 2 and 3). This implies that, although some additional dynamic quenching processes occur within an oligo, the substantial portion of the loss of fluorescence intensity is due to static quenching interactions. To show this difference between the steady-state and time-resolved fluorescence parameters in

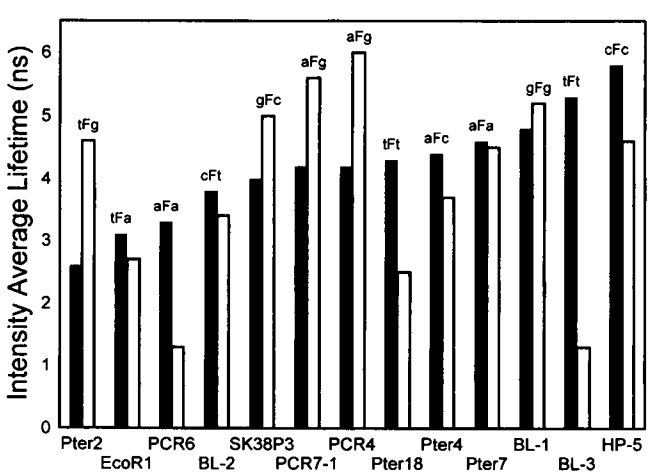

FIGURE 5 The intensity average lifetimes (Table 3) for the ss (*solid bars*) and ds (*open bars*) oligos, arranged by increasing magnitude for the ss oligos. Each oligo is labeled with the three nucleotides centered around the 3-MI probe depicted by F.

another way, the ratios of the number-average lifetimes to the corresponding relative quantum yields were calculated and are listed in Table 4. If it is assumed that this ratio for 3-MI in solution represents only dynamic quenching processes, then ratios above 6.5 depict the presence of static quenching conferred by interactions with the oligonucleotide. This ratio for those ss oligos without a purine either 5′ or 3′ of 3-MI is similar to that for 3-MI, suggesting that little static quenching occurs when the nearest neighbors are both pyrimidines. However, when a purine is either 5′ or 3′ of the probe, then a significantly higher ratio is observed for the ss oligos. In analogy with the quantum yield results, the ratio for a 3′ purine is larger than for a 5′ purine, suggesting that the interaction leading to static quenching is favored when the purine follows the 3-MI probe in the sequence. The largest ratios are found for those oligos with a purine on both sides of 3-MI, excluding the as yet unexplained exception of PCR6.

For most samples, this ratio increased upon formation of the ds oligo. A larger increase appeared to be associated with those oligos having a purine next to the probe. This increase suggests that the lower fluorescence quantum yields seen with the ds oligos are also primarily a result of static quenching interactions, especially as the average lifetimes for some of the ss oligos actually increased on formation of the ds oligo. The further quenching of 3-MI could be a result of additional interactions with the complement nucleotide strand. In addition, quenching interactions could be enhanced with components of its own strand due to new structural constraints following formation of the double helix. For example, the ds environment could alter the equilibrium and thus increase the probability of forming a ground-state, statically quenched complex. For three oligos, EcoR1, Pter4, PCR6, and perhaps Pter7, the ratio decreased for the ds compared with the ss oligo. One possible explanation for this observation would be that formation of the ds oligo actually hinders the formation of ground-state complexes responsible for static quenching.

TABLE 4 Comparison of number-average lifetimes and relative quantum yields

	$\bar{\tau}/\Phi^{\#}$	
Sample*	ss	ds
3-MI	6.5	
Pter18	9.4	23
BL-3	7.7	11.7
BL-2	10.6	62
HP-5	14.4	129
EcoR1	33	20
Pter2	49	300
Pter4	26	16.7
SK38P3	30	194
Pter7	200	140
PCR6	32	7.7
PCR4	52	267
PCR7-1	106	383
BL-1	106	517

*Samples grouped by nearest neighbors; see Table 2.
#The number-average lifetime (Table 3) divided by the relative quantum yield (Table 2).

It therefore appears that a majority of the loss in quantum yield results from formation of a ground-state complex between the nucleotide analog and one or more elements of the oligo. This complex then acts as a static quencher. In the ss samples, the efficiency of complex formation, the static quenching mechanism, or both, is favored when a purine is immediately 5′ or 3′ of 3-MI. If there is a purine both 5′ and 3′ of 3-MI, the quenching effect is enhanced. The major contribution to the further loss of fluorescence intensity for the ds oligos is also static quenching. More studies are obviously required to help elucidate the nature of these static quenching effects. Questions to be addressed include whether there is a difference between adenine and guanine as the 5′ or 3′ neighboring purine, as suggested by the quantum yield data, and whether these interactions also contribute to the complex fluorescence intensity decay kinetics. The latter possibility stems from the observation that the only large variations in the intensity decay parameters between the different oligos, and between ss and ds oligos, were with the amplitudes. Such variations could suggest a shift in equilibrium populations between a ground-state complex required for static quenching and an environment where the quenching group dynamically interacts with 3-MI.

Additional characterizations

Two other experimental approaches have been used to help evaluate the usefulness of 3-MI as a fluorescent nucleotide analog. The first, quenching by an added solute, quickly proved its inability to provide any information. The second, time-resolved anisotropy, has yielded only hints of relevant information due to questions regarding the appropriate mathematical function to use for data analysis. The details of both approaches are highlighted below.

Steady-state and time-resolved fluorescence quenching experiments were performed, using acrylamide to avoid electrostatic interactions, to evaluate the accessibility of solvent to 3-MI as well as to provide information about interactions between 3-MI and its neighboring nucleotides. The data (not shown) for the quenching of 3-MI in buffer revealed some interesting and unexpected results. First, an upward curving steady-state Stern-Volmer plot denoted the presence of static quenching (Eftink and Ghiron, 1981; Laws and Contino, 1992) due to a ground-state complex between 3-MI and acrylamide; acrylamide has been previously shown to form static quenching complexes with a variety of fluorophores (Eftink and Ghiron, 1981; Casali et al., 1990; Contino and Laws, 1991). Second, there is very little dynamic quenching as demonstrated by a k_q of 1×10^8 M^{-1} s^{-1}, which is an order of magnitude less than that expected for small, well solvated molecules (Eftink and Ghiron, 1981). Third, similar steady-state and time-resolved results were observed for DMI (see Fig. 1), implying that the ribose ring does not shield the isoxanthopterin ring from

dynamic interactions with solutes. Consequently, the inability of acrylamide to quench 3-MI (or DMI) in solution by a dynamic interaction remains unresolved. Even more intriguing was the finding that neither dynamic nor static quenching was occurring with the ss oligos EcoR1 and Pter18. As the results above indicated the existence of ground-state complexes leading to static quenching, the inability to quench 3-MI in a ss oligo is likely due to steric hindrance. Based on these results, no attempt was made to perform quenching experiments with ds samples. In analogy with the absorption and emission spectra, quenching by acrylamide does not appear to be a way to assess the local environment of 3-MI in an oligo. More experiments will have to be done, however, as it is conceivable that other agents besides acrylamide may be able to dynamically quench 3-MI and thus help define its environment in an oligo.

Time-resolved fluorescence anisotropy experiments were performed for all samples. The anisotropy decay of 3-MI in buffer can be described by a single rotational correlation time near 80 ps. However, a time nearer 50 ps might be expected, assuming that 3-MI is a sphere of a radius estimated from its most extended conformation. To help resolve this difference, 3-MI was modeled by a set of spheres representing the carbons, nitrogens, and oxygens, and the hydrodynamic parameters of this object were calculated using the program HYDRO (Garcia de la Torre et al., 1994). Three conformations were examined: 1) stacked deoxyribose and isoxanthopterin rings, 2) extended with coplanar rings, and 3) extended with orthogonal rings. When four spheres representing water molecules hydrogen bonded to 3-MI were included, the calculated correlation times for the extended orthogonal conformation were in the range of 70–90 ps. Although this modeling is not conclusive, it suggests that a rotational correlation time of 80 ps for 3-MI in water is reasonable.

The excitation and emission dipoles of 3-MI appear to be nearly parallel. The β term for the anisotropy decay of 3-MI obtained with 323 and 335 nm excitation, 0.38, is close to the theoretical maximum of 0.4 for the anisotropy at time 0 (r_o). In addition, these values agree with the principle polarization spectrum for 3-MI dissolved in glycerol (Fig. 6), which indicates that the low-energy absorption band consists of a single transition with a limiting $\langle r \rangle$ near 0.39.

For a comparison with 2-AP-containing oligos, fluorescence anisotropy decay experiments were also conducted on all of the ss and ds forms of the oligos listed in Table 1. Unfortunately, none of the data sets have been analyzed satisfactorily. If an analysis was able to yield acceptable fits for all three decay curves ($I_m(t)$, $I_v(t)$, and $I_h(t)$), then one or more of the iterated parameters had values that were not physically relevant. For example, the sum of the β_j terms (r_o) was >0.4 and/or the longest rotational correlation time was >100 ns. If all parameters were set to reasonable values, then unacceptable fits were observed. This occurs even when the α_i and τ_i terms for $I_m(t)$ were determined first and then held constant during the iterations for the r(t) parameters.

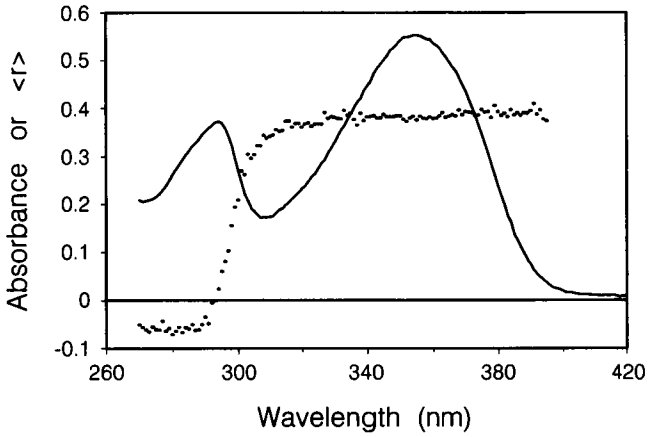

FIGURE 6 The absorbance (——) and principle polarization (· · ·) spectra for 3-MI dissolved in glycerol.

The inability to analyze these data sets appears to be a direct consequence of using an inappropriate mathematical function to model the anisotropy decay. For lack of a better model, each lifetime component of the intensity decay has been linked to each of the rotational correlation times. This model, however, assumes that each lifetime is the result of a specific, resolvable kinetic event. As we do not know the kinetic mechanism describing the time-dependent loss of fluorescence intensity, and have only fit the data to an arbitrary sum of exponentials, we do not know what each lifetime represents. To analyze the anisotropy decay of these 3-MI-containing oligos, the kinetic mechanism describing the fluorescence intensity decay must first be determined, and then the correct linkages between intensity decay events and depolarization events must be found.

Despite the inability to resolve the anisotropy decay of these oligos, certain general information concerning the dynamic motions of the 3-MI probe in an oligo can be deduced from the analyses. In most cases, three correlation times were required: two short (≤1 ns) ones and one representing that expected for the global rotation of the oligo (≥10 ns). The magnitude of the short correlation times are indicative of depolarizing motions involving the 3-MI probe independent of the rest of the oligo. Based on the harmonic mean correlation time ($\langle \phi^{-1} \rangle = [\Sigma\beta_j/\phi_j]/\Sigma\beta_j$), these rapid motions dominate the depolarization process. This is observed even in the ds samples, which suggests that the 3-MI probe is still able to undergo independent motions leading to the depolarization of fluorescence in the ds samples as freely as in the ss samples. As 3-MI is unable to make hydrogen bonds exactly analogous to guanine, it is possible that its presence introduces a perturbation into the structure of the DNA at that location. As a result, the 3-MI probe could have as much freedom of independent motion on the nanosecond time scale in the ds as in the ss samples. This altered structure interpretation is supported by the observation that the melting temperatures for 3-MI-containing ds oligos are lower than guanosine-containing control samples

(Hawkins et al., 1997). In contrast, the similar anisotropy decay parameters previously observed for 2-AP in oligos (Nordland et al., 1989; Guest et al., 1991), which does base pair normally, could suggest that nucleotide bases have a substantial amount of dynamic motion in an oligo, independent of base pairing, leading to the depolarization of the excited state. It is also possible that these rapid correlation times are related to the process or processes depopulating the excited state, for example, an excited-state reaction leading to a perturbation in the emission dipole moment and thus a depolarization, and do not actually reflect on dynamic motions of the fluorescent base analog. It is therefore imperative that the basic decay mechanism be worked out to enable the full use of these nucleotide analogs for the study of protein-DNA complexes.

We thank Dr. Ronald Kohanski for the use of his FPLC and MonoQ column that we used to establish the purification protocol, Dr. Donald Senear for advice on annealing and purification, Dr. Jose Garcia de la Torre for the code to HYDRO, and Dr. J.B. Alexander Ross and Mr. Edward Rachofsky for discussions on data analysis.

This work was supported in part by National Institutes of Health grant GM39750. S.L. Driscoll was a 1995 Sigma Xi-Rudin Foundation Summer Fellow.

REFERENCES

Badea, M. G., and L. Brand. 1979. Time-resolved fluorescence measurements. *Methods Enzymol.* 61:378–425.

Beechem, J. M., and L. Brand. 1979. Time-resolved fluorescence of proteins. *Annu. Rev. Biochem.* 54:43–71.

Bevington, P. R. 1969. Data Reduction and Error Analysis for the Physical Sciences. McGraw-Hill, New York. 204–246.

Brown, T., and D. J. S. Brown. 1991. Oligonucleotides and Analogues: A Practical Approach. F. Eckstein, editor. Oxford University Press, New York. 1–24.

Cantor, C. R., and P. R. Schimmel. 1980. Biophysical Chemistry. Chap. 7. W. H. Freeman Co., San Francisco.

Casali, E., P. H. Petra, and J. B. A. Ross. 1990. Fluorescence investigation of the sex steroid binding protein of rabbit serum: steroid and subunit dissociation. *Biochemistry.* 29:9334–9343.

Contino, P. B., and W. R. Laws. 1991. Rotamer-specific fluorescence quenching in tyrosinamide: dynamic and static interactions. *J. Fluoresc.* 1:5–13.

Eftink, M. R. 1991. Fluorescence techniques for studying protein structure. *Methods Biochem. Anal.* 35:127–205.

Eftink, M. R., and C. A. Ghiron. 1981. Fluorescence quenching studies with proteins. *Anal. Biochem.* 114:199–227.

Garcia de la Torre, J., S. Navarro, M. C. Lopez Martinez, F. G. Diaz, and J. J. Lopez Cascales. 1994. HYDRO: a computer program for the prediction of hydrodynamic properties of macromolecules. *Biophys. J.* 14:81–139.

Grinvald, A., and I. Z. Steinberg. 1974. On the analysis of fluorescence decay kinetics by the method of least squares. *Anal. Biochem.* 59: 583–598.

Guest, C. R., R. A. Hochstrasser, L. C. Sowers, and D. P. Millar. 1991. Dynamics of mismatched base-pairs in DNA. *Biochemistry.* 30: 3271–3279.

Hasselbacher, C. A., E. Waxman, L. T. Galati, P. B. Contino, J. B. A. Ross, and W. R. Laws. 1991. Investigation of hydrogen bonding and protein transfer of aromatic alcohols in nonaqueous solvents by steady-state and time-resolved fluorescence. *J. Phys. Chem.* 95:2995–3005.

Hawkins, M. E., W. Pfleiderer, F. M. Balis, D. Porter, and J. R. Knutson. 1997. Fluorescence properties of pteridine nucleoside analogs as monomers and incorporated into oligonucleotides. *Anal. Biochem.* 244:86–95.

Hawkins, M. E., W. Pfleiderer, A. Mazumder, Y. G. Pommier, and F. M. Balis. 1995. Incorporation of a fluorescent guanosine analog into oligonucleotides and its application to a real time assay for the HIV-1 integrase 3′-processing reaction. *Nucleic Acids Res.* 23:2872–2880.

Hochstrasser, R. A., T. E. Carver, L. C. Sowers, and D. P. Millar. 1994. Melting of a DNA helix terminus within the active site of a DNA polymerase. *Biochemistry.* 33:11971–11979.

Hogue, C. W. V., I. Rasquinha, A. G. Szabo, and J. P. MacManus. 1992. A new intrinsic fluorescent probe for proteins: Biosynthetic incorporation of 5-hydroxytryptophan into oncomodulin. *FEBS Lett.* 310: 269–272.

Konev, S. V. 1967. Fluorescence and Phosphorescence of Proteins and Nucleic Acids. Plenum Press, New York.

Lakowicz, J. R. 1983. Principles of Fluorescence Spectroscopy. Plenum Press, New York.

Laws, W. R., and P. B. Contino. 1992. Fluorescence quenching studies: analysis of nonlinear Stern-Volmer data. *Methods Enzymol.* 210: 448–463.

Nordlund, T. M., S. Andersson, L. Nilsson, R. Rigler, A. Gräslund, and L. W. McLaughlin. 1989. Structure and dynamics of a fluorescent DNA oligomer containing the EcoR1 recognition sequence: fluorescence, molecular dynamics, and NMR studies. *Biochemistry.* 28:9095–9103.

Pfleiderer, W., and M. Rukwied. 1961. Pteridines. XI. The structure of isoxanthopterin. *Chem. Ber.* 94:1–12.

Ross, J. B. A., D. F. Senear, E. Waxman, B. B. Kombo, E. Rusinova, Y. T. Huang, W. R. Laws, and C. A. Hasselbacher. 1992. Spectral enhancement of proteins: biological incorporation and fluorescence characterization of 5-hydroxytryptophan in bacteriophage lambda cI repressor. *Proc. Natl. Acad. Sci. U.S.A.* 24:12023–12027.

Ross, J. B. A., A. G. Szabo, and C. W. V. Hogue. 1997. Enhancement of protein spectra with tryptophan analogues: fluorescence spectroscopy of protein-protein and protein-nucleic acid interactions. *Methods Enzymol.* 278:151–190.

Stern, O., and M. Volmer. 1919. On the quenching-time of fluorescence. *Physik. Zeitschr.* 20:183–188.

Waxman, E., W. R. Laws, T. M. Laue, Y. Nemerson, and J. B. A. Ross. 1993. Human factor VIIa and its complex with soluble tissue factor: evaluation of asymmetry and conformational dynamics by ultracentrifugation and fluorescence anisotropy decay methods. *Biochemistry.* 32: 3005–3012.